Sub-regional Pattern Analysis of Heterogeneous PET Tracer Distribution Employed for Disease Assessment

Ivan S. Klyuzhin*, Jessie Fu*, Nikolay Shenkov*, Arman Rahmim†, Vesna Sossi*
* Department of Physics and Astronomy, University of British Columbia, Vancouver, BC, V6T1Z1; Email: ivansk@physics.ubc.ca
† Department of Radiology, Johns Hopkins University, Baltimore, MD 21287

***Abstract*—The mean value of the non-displaceable binding potential (BP_{ND}) within a region of interest (ROI) is the traditionally-employed metric in neurological image analysis. The ability of the mean value to accurately track clinical disease progression may be limited since it does not capture the spatial pattern of tracer distribution. In this work, we employ the principal component analysis (PCA) to quantify the clinically-relevant tracer binding patterns ([11C]dihydrotetrabenazine) in high-resolution PET images of 37 Parkinson's disease subjects. The principal component (PC) scores that correspond to different binding patterns in the putamen ROIs are combined with the mean BP_{ND} and used as the input to several linear models that aim to predict the clinical severity of the disease (disease duration). Multiple regression analysis and LASSO (least absolute shrinkage and selection operator) with cross-validation are used to evaluate the contributions of the PC scores to the accuracy of the tested models. With multiple regression analysis, the value of the adjusted R^2 was 0.57 when the mean BP_{ND} alone was used as the model input. When the PC scores were included as additional input variables, the value of the adjusted R^2 increased to 0.70. The terms of the model representing the PC scores were statistically significant ($p<0.01$). In LASSO analysis, the cross-validated accuracy improved by 25% when the PC scores were added to the input (compared to using the mean BP_{ND} alone). These results demonstrate that a) the disease- and tracer-specific binding patterns can be identified in sub-cortical brain structures from high-resolution PET images, and b) such patterns may facilitate better models of the clinical disease metrics.**

I. Introduction

Disease-induced physiological changes in the brain often manifest in a distinct spatio-temporal pattern of tracer binding. On the other hand, metrics traditionally used in neurological image analysis (e.g. the non-displaceable binding potential - BP_{ND}) are often estimated from the mean voxel value inside a region of interest (ROI). The ability of the mean value to track clinical disease progression may be limited in terms of accuracy and sensitivity to subtle changes, since it does not capture the spatial pattern of tracer distribution. It was previously demonstrated that geometry [1] and texture [2], [3], [5] metrics that quantify spatial patterns, such as Haralick features [6]–[8] and moment invariants [4], exhibit significant correlations with the clinical severity of Parkinson's disease (PD). Nevertheless, the practical utility of such metrics remained questionable since the measured correlation values were lower than that of the mean BP_{ND}. In this work, we explore a different approach to spatial pattern quantification. The (structure- and disease-specific) sub-regional patterns of the tracer distribution in the putamen are identified by performing the principal component analysis (PCA) on high-resolution PET images. The principal component (PC) scores are combined with the mean BP_{ND} or activity ratio (AR) and used as the input variables to several linear models that aim to predict the clinical measure - PD duration - for the imaged subjects (PD severity increases with time). We evaluate the contribution of the PC scores to the accuracy of the tested models utilizing two different regression methods and 5-fold cross-validation. We demonstrate that highest accuracy is achieved when the mean ROI value is combined with the PC scores that quantify the prevalence of specific tracer binding patterns inside the ROI.

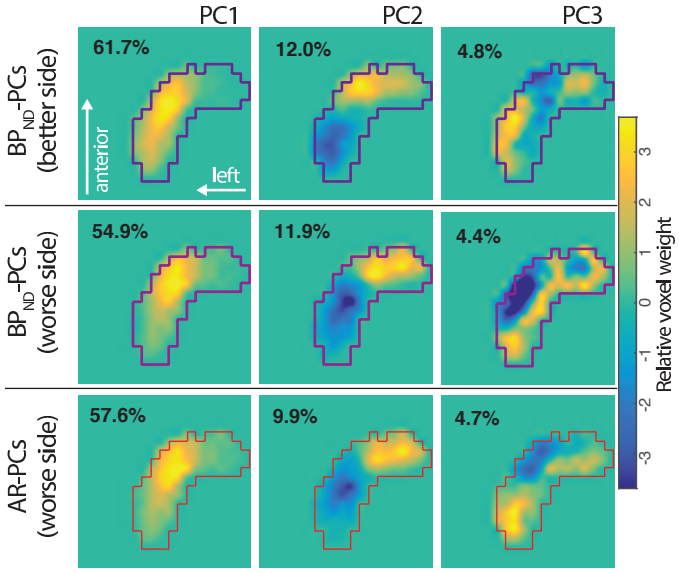

Fig. 1. PCs obtained from the analysis of BP_{ND} and AR images of the putamen (outlined contour), computed in the better (less affected) and worse sides. Numbers represent the percent of total variance explained.

II. Methods

A. Data acquisition and pre-processing

Dynamic PET images of [11C]dihydrotetrabenazine (DTBZ, a marker of the vesicular dopamine transporter

type 2) were obtained using the high-resolution research tomograph (HRRT, Siemens) for 37 PD subjects. T1W-MRI images were acquired and co-registered with the PET images. DTBZ BP_{ND} and AR (voxel activity averaged over the 30-60 min post-injection time interval divided by the mean activity in the reference region) images were computed from the reconstructed activity concentration images. Subcortical segmentation of the MRI images was performed using Freesurfer. The ROIs comprising the left and right putamen for each subject were warped to a common putamen ROI using 3D diffeomorphic mapping, and the resulting transformation was applied to the BP_{ND} and AR images. Each voxel in the common putamen ROI was treated as a variable, and voxel values (BP_{ND} or AR) corresponding to different subjects were treated as observations. PCA was performed on these data. Two sets of PCs were computed using the BP_{ND} values from the better (less affected by the disease) and worse sides (BP_{ND}-PCs), and similarly two other sets of PCs were computed using the AR values (AR-PCs) from the respective sides.

B. Analysis methods

We evaluated the goodness of fit and the cross-validated accuracy of several linear models, where the PD duration was the dependent variable, and the mean ROI values combined with PC scores were the independent variables. The PC scores were computed as the dot product between the voxel weights in the PC and the vector of voxel values: B_N^{BP} (W_N^{BP}), $N = 1, 2, ...$, denotes the score for the N-th PC computed on the better (worse) side using BP_{ND}-PCs and the BP_{ND} voxel values; B_0^{BP} denotes the mean value of BP_{ND}. The same notation is used for the metrics computed from the AR images (e.g. B_0^{AR}).

Two methods of regression analysis were employed. In the first method, we chose a subset of the input variables (either BP_{ND} or AR-based) from the better and worse sides based on the prior knowledge of the disease progression pattern. For each tested model, we measured the individual variable p-values and the adjusted R^2_{adj} of the fit. In the second method, we used LASSO for variable selection and regression. All variables (4 per side, 8 in total) were used in the LASSO input, and the method eliminated some of the variables as the regularization parameter λ was gradually increased from 0 to 1. The accuracy of models corresponding to different λ was measured using the cross-validated mean squared error (MSE, measured in the test subset) between the estimated and ground truth PD duration. The importance of different variables in the best model was evaluated based on the magnitude of their fitting coefficients.

III. Results

A. PCA-derived patterns

The first 3 PCs accounting for most variance in different PC sets are visualized in Fig. 1. The first components represent the weighted mean of voxel values in the region; since this is similar to the ROI-mean voxel value, the mean values B_0 and W_0 were used in place of B_1 and W_1 in the regression analysis. Patterns revealed by PC2 are interpreted as quantifying the posterior-anterior gradient of the dopaminergic terminal loss, and the following PCs are more difficult to interpret. Only the first 4 PCs were used in the regression analysis, since the pattern of PC5 and onwards strongly resembled random noise. PCs computed on the better side differ from PCs computed on the worse side. For example, on the worse side, the boundary between the positive and negative regions in PC2 is shifted in the anterior direction. Using the BP_{ND} and AR images for PCA also resulted in different patterns even for the same side, particularly in PC3 and PC4.

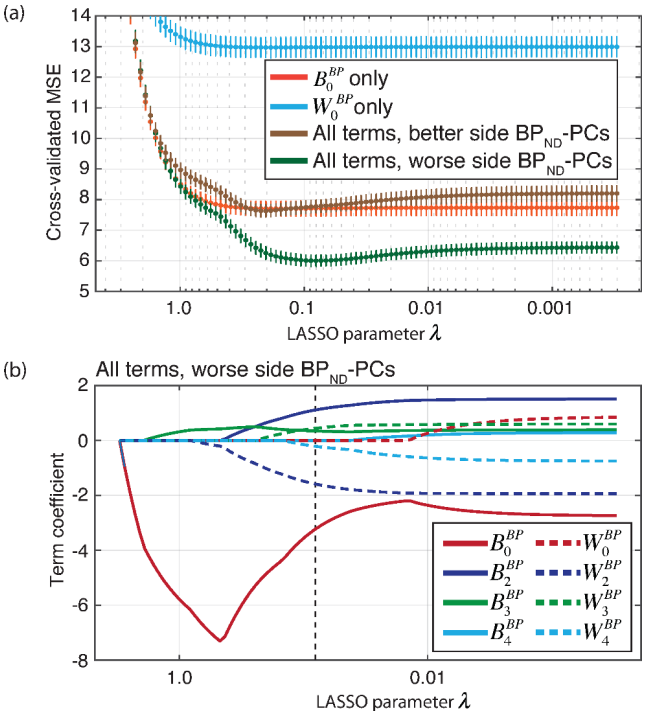

Fig. 2. (a) The MSE of models plotted against the LASSO regularization parameter λ. 50 repetitions of 5-fold cross-validation were performed to obtain the plotted means and standard deviations. Legend specifies variables in the input to LASSO. (b) Variable coefficients in the best model plotted against λ. Higher λ corresponds to greater regularization. Dashed vertical line marks the λ corresponding to the lowest MSE.

B. Regression analysis

The values of R^2_{adj} obtained with tested linear models are given in Table I. Generally, combining the metrics from the better and worse sides resulted in higher correlation coefficient, especially with the AR-derived metrics. The term W_0^{BP} became insignificant whenever B_0^{BP} was included in the regression; however, the terms $W_2^{BP} - W_4^{BP}$ remained significant.

C. LASSO analysis

The cross-validated MSE is plotted as a function of the λ parameter in Fig. 2a, for 4 combinations of the input variables. The input consisting of only B_0^{BP} or W_0^{BP} represent the reference models. The graph demonstrates that the inclusion of

TABLE I
RESULTS OF THE MULTIPLE REGRESSION ANALYSIS.

Included terms (AR)	R^2_{adj}	Included terms (BP)	R^2_{adj}
$\{B_0^{AR*}\}$	0.31	$\{B_0^{BP*}\}$	0.57
$\{W_0^{AR}\}$	0.07	$\{W_0^{BP*}\}$	0.24
$\{B_0^{AR*}, W_0^{AR*}\}$	0.44	$\{B_0^{BP*}, W_0^{BP}\}$	0.58
$\{B_0^{AR*}, W_0^{AR*}, W_4^{AR*}\}$	**0.53**	$\{B_0^{BP*}, B_3^{BP*}, W_3^{BP*}\}$	**0.70**

* Terms with p<0.01.

PC scores (B_N^{BP} and W_N^{BP}) computed using the PCs from the better side did not reduce the MSE compared to the reference. A significant reduction of the MSE ($\sim$25%) was achieved using the PCs derived from the worse side. The trace plot of the term coefficients of the best model (Fig. 2b) demonstrates that the terms B_4^{BP}, W_0^{BP} and W_4^{BP} were eliminated first with $\lambda \to 1$. The best accuracy was achieved with non-zero terms B_0^{BP}, W_2^{BP}, B_2^{BP}, B_3^{BP} and W_3^{BP}.

IV. CONCLUSIONS

The new method of sub-regional pattern analysis explored in this work revealed several important trends and correlations in the data that are specific to DTBZ imaging of PD subjects. Specifically, the results demonstrate that both sides of the striatum contain non-redundant information relevant to the disease (only one side was used in the previous studies). On the more affected side, the spatial pattern of tracer distribution carries more information than the mean voxel value - however, only in the case if the better side mean is included in the model. This new information will contribute to the image analysis methodology in future PD imaging studies. More generally, the results demonstrate that a) the disease- and tracer-specific binding patterns can be identified in sub-cortical brain structures using high-resolution PET imaging, and b) such patterns may facilitate better models of the clinical disease metrics. We believe that the method of analysis described here can be applied to a variety of studies that utilize different tracers and focus on different pathologies and disorders.

REFERENCES

[1] Klyuzhin, I., et al. (2016). Exploring the use of shape and texture descriptors of positron emission tomography tracer distribution in imaging studies of neurodegenerative disease. J. Cereb. Blood Flow Metab., vol. 36, no. 6, pp. 112234.

[2] Rahmim, A., et al. (2016). Application of texture analysis to DAT SPECT imaging: Relationship to clinical assessments. NeuroImage: Clinical. http://doi.org/10.1016/j.nicl.2016.02.012

[3] Klyuzhin, I., et al. (2015). Investigation of the Texture Quantification Parameters for Neurological PET Image Analysis. In 2015 IEEE NSS/MIC conference record. San Diego, CA: IEEE.

[4] Gonzalez, M. E. et al. (2013). Novel spatial analysis method for PET images using 3D moment invariants: Applications to Parkinsons disease. Neuroimage, vol. 68, pp. 1121.

[5] Blinder, S. A. L., et al. (2014). Texture and Shape Analysis on High and Low Spatial Resolution Emission Images. In 2014 IEEE NSS/MIC conference record (NSS/MIC). Seattle, WA: IEEE.

[6] Martinez-Murcia, F. J., et al. (2014). Parametrization of textural patterns in 123I-ioflupane imaging for the automatic detection of Parkinsonism. Med. Phys., vol. 41, no. 1, p. 012502.

[7] Haralick R. M., Shanmugam, K., Dinstein, I. (1973). Textural Features for Image Classification. IEEE Trans. Syst. Man. Cybern., vol. 3, no. 6, pp. 610621.

[8] Soh, L.-K., Tsatsoulis, C. (1999). Texture analysis of SAR sea ice imagery using gray level co-occurrence matrices. IEEE Trans. Geosci. Remote Sens., vol. 37, no. 2, pp. 780795.